

Radiative-emission analysis in charge-exchange collisions of O⁶⁺ with argon, water, and methane

Anthony C. K. Leung* and Tom Kirchner†

Department of Physics and Astronomy, York University, Toronto, Ontario, Canada M3J 1P3

(Received 6 March 2017; published 10 April 2017)

Processes of electron capture followed by Auger and radiative decay were investigated in slow ion-atom and -molecule collisions. A quantum-mechanical analysis which utilizes the basis generator method within an independent electron model was carried out for collisions of O⁶⁺ with Ar, H₂O, and CH₄ at impact energies of 1.17 and 2.33 keV/amu. At these impact energies, a closure approximation in the spectral representation of the Hamiltonian for molecules was found to be necessary to yield reliable results. Total single-, double-, and triple-electron-capture cross sections obtained show good agreement with previous measurements and calculations using the classical trajectory Monte Carlo method. The corresponding emission spectra from single capture for each collision system are in satisfactory agreement with previous calculations.

DOI: [10.1103/PhysRevA.95.042703](https://doi.org/10.1103/PhysRevA.95.042703)**I. INTRODUCTION**

Numerous efforts have been made in recent years to gain a deeper understanding of radiative emissions from slow (a few keV/amu or less) ion-atom and -molecule collisions [1–5]. Studies of these slow collision systems are important for understanding the large production of photoemissions in astrophysical settings. A prime example is the interaction between highly charged solar wind ions and cometary gases [6], where charge exchange is the main mechanism for the observed emissions [7].

With the composition known [8], one can study such interactions in the laboratory or theoretically. In fact, atomic data obtained from such studies are deemed important by the astrophysics community [9–11]. Together with x-ray satellite measurements, these capture cross sections can be useful in deducing solar wind ion abundances [12].

Slow collision systems in astrophysical settings are also of significant interest from the perspective of fundamental physics. With numerous measurements reported in the past decade, one can compare these measurements with theoretical models such as the classical-trajectory Monte Carlo (CTMC) method [13] or quantum-mechanical close-coupling approaches [14].

A recent experiment by Machacek *et al.* [15] reported capture cross sections from collision systems at 1.17 and 2.33 keV/amu impact energies involving O⁶⁺ ions with neutral Ar and several molecules, including H₂O and CH₄ vapor, species relevant to the cometary emission phenomenon. These impact speeds represent the slow and fast solar wind speeds, respectively. CTMC calculations of these cross sections were also performed and compared with the measurements. While there was satisfactory agreement in total single-electron capture (SEC) and total double-electron capture (DEC), triple-electron-capture (TEC) results were underestimated by theory. With only predicted spectra based on the CTMC method reported, it is worthwhile to examine this problem using more elaborate methods from quantum-mechanical approaches for confirmation.

In this article, we present results of such an analysis for a selected number of collision systems that were investigated by Machacek *et al.* [15]. Specifically, the present analysis examines and compares the radiative-emission spectra produced from O⁶⁺-Ar, -H₂O, and -CH₄ collision systems at 1.17 and 2.33 keV/amu impact energies. Given the first ionization energy of Ar (15.75 eV) is rather close to that of H₂O (12.62 eV) and CH₄ (12.61 eV), by the classical over-barrier model (OBM) [16,17] it is expected that the main capture channel on the projectile is identical for all targets.

The present analysis is based on the independent-electron model (IEM) using the nonperturbative two-center basis generator method (TC-BGM) [18]. The TC-BGM is a coupled-channel approach which uses a dynamically adapted basis to reach convergence rather than a very large basis set. This method has been used to describe a variety of collision systems and their applications [19–22], including the relevant cometary emission phenomenon [23–25]. In recent studies, the TC-BGM was adapted for ion-molecule collisions [26] to describe electronic processes in water- and methane-vapor targets at higher impact energies [27–29]. Given that we have yet to explore the TC-BGM for ion-molecule collisions at low impact energies, the data reported by Machacek *et al.* [15] serve as an excellent benchmark to guide the present models.

The following describes how the article is organized. In Sec. II, we provide an overview of the TC-BGM for ion-atom and ion-molecule collisions in the framework of the IEM. In Sec. III, results of the analysis are presented and compared with previous studies. Results of capture cross sections are discussed in Sec. III A followed by the radiative spectra in Sec. III B. Last, we provide our concluding remarks in Sec. IV. Atomic units ($\hbar = e = m_e = 4\pi\epsilon_0 = 1$) are used throughout the article unless stated otherwise.

II. THEORETICAL METHODS**A. Collision dynamics**

The theoretical treatment for all collision systems in this study utilizes the semiclassical approximation where the target (T) core is centered at the origin and the O⁶⁺ projectile (P) travels at constant speed v_P in a straight path described by $\mathbf{R}(t) = (b, 0, v_P t)$, where b is the impact parameter. Then, \mathbf{r}_T

*leungant@yorku.ca

†tomk@yorku.ca

and $\mathbf{r}_p = \mathbf{r}_T - \mathbf{R}(t)$ are the positions of the target electron with respect to the target and projectile cores, respectively. While the approach for both atomic and molecular targets utilizes the TC-BGM in the IEM framework, there are particular differences in the treatment of these two types of targets.

1. Ion-atom collisions

Within the IEM, the ion-atom collision problem is represented by the single-particle time-dependent Schrödinger equation (TDSE)

$$i \partial_t |\psi_i(t)\rangle = \hat{h}(t) |\psi_i(t)\rangle, \quad (1)$$

where \hat{h} is the single-particle Hamiltonian

$$\hat{h} = -\frac{1}{2}\Delta + V^P + V^T. \quad (2)$$

The potential of the O^{6+} projectile, $V^P = V^{O^{6+}}$, is represented by the model potential [14]

$$V^{O^{6+}}(r_p) = -\frac{6}{r_p} - \frac{2}{r_p} \exp(-2\alpha r_p)(1 + 2\alpha r_p + 2\alpha^2 r_p^2), \quad (3)$$

with $\alpha = 8.4$. The neutral argon target $V^T = V^{Ar}$ is represented by the potential

$$V^{Ar}(r_T, t) = -\frac{18}{r_T} + v_{ee}(r_T, t), \quad (4)$$

where v_{ee} is an effective mean-field potential that models the screening and electron-exchange interaction. We consider two variants of this model: (i) the *no-response* approximation, in which we utilized the exchange-only version of the optimized potential method of ground-state density functional theory [30], and (ii) a *target-response* model, which includes a time-dependent screening potential due to electron removal during the collision. The formulation of this response model and a discussion of its importance towards total capture for slow-collision problems can be found in Ref. [31].

The single-particle equations for the Hamiltonian (2) are solved using the TC-BGM. The basis for the O^{6+} -Ar system consists of the LMN shells of the target (K -shell electrons were assumed to be frozen), all nlm states from $n = 2$ to $n = 6$ on the O^{5+} projectile, and a set of TC-BGM pseudostates to account for ionization and intermediate quasimolecular couplings.

2. Ion-molecule collisions

An elaborate formulation and discussion of the TC-BGM adaptation for ion-molecule collision problems is given in Ref. [27]. For this reason, only a brief summary highlighting the key techniques is provided here.

Similar to the ion-atom collision problem, we address the ion-molecule problem within the IEM. The objective for the ion-molecule problem is to solve a set of single-particle TDSEs

$$i \partial_t |\psi_{\alpha\beta\gamma}^\Gamma(t)\rangle = \hat{h}_{\alpha\beta\gamma}(t) |\psi_{\alpha\beta\gamma}^\Gamma(t)\rangle \quad (5)$$

for the initial conditions

$$|\psi_{\alpha\beta\gamma}^\Gamma(t_i)\rangle = |\Gamma_{\alpha\beta\gamma}\rangle, \quad (6)$$

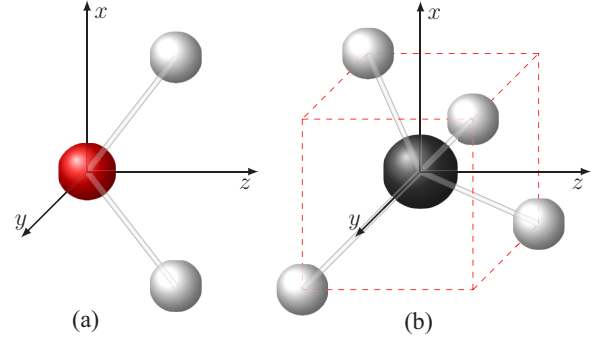


FIG. 1. Original orientation $(\alpha, \beta, \gamma) = (0, 0, 0)$ of the molecules considered: (a) H_2O , where the oxygen atom is at the origin with the two hydrogen atoms situated in the collision xz plane [32], and (b) CH_4 , where the carbon atom is at the origin [33]. The cube drawn with dashed lines and centered at the origin helps visualize the geometry of CH_4 .

where $|\Gamma_{\alpha\beta\gamma}\rangle$ are the initially occupied molecular orbitals and the parameters α , β , and γ are the Euler angles (in degrees) that define the molecular orientation with respect to the ion-beam axis. The original coordinate system, $(\alpha, \beta, \gamma) = (0, 0, 0)$, for H_2O and CH_4 and information on the corresponding molecular orbitals on the Hartree-Fock level are taken from Refs. [32,33], respectively. This orientation for both molecules is shown in Fig. 1. By applying a rotation operator on states corresponding to the original coordinate system, one obtains a rotated basis representing a different orientation for which a new set of collision calculations can be carried out.

Due to the fact that the xz plane is chosen to be the scattering plane for the present method, we can select only molecular orientations in which the system is invariant under a reflection with respect to this plane. Although six orientations were initially considered for H_2O , it turns out that it is sufficient to carry out total cross-section calculations for just two orientations, namely, $(0, 0, 0)$ and $(90, 0, 0)$. The same finding was also seen in Refs. [26,27]. For CH_4 , four orientations were considered: $(0, 0, -45)$, $(0, -90, -45)$, $(45, 90, 180)$, and $(-45, -90, 0)$ [29].

We express the Hamiltonian in Eq. (5) as

$$\hat{h}_{\alpha\beta\gamma} = \hat{h}_{\alpha\beta\gamma}^T + V^P, \quad (7)$$

where $\hat{h}_{\alpha\beta\gamma}^T$ is an effective Hartree-Fock Hamiltonian of the target and V^P is the interaction potential with the O^{6+} projectile (3). As discussed in previous works [26,27], the main difficulty in solving the single-particle TDSE for the molecular problem (5) is the occurrence of multicenter matrix elements. The strategy is to avoid the explicit calculation of multicenter integrals, and this involves two ideas: (i) expressing $\hat{h}_{\alpha\beta\gamma}^T$ in its spectral representation

$$\hat{h}_{\alpha\beta\gamma}^T = \sum_{\Lambda} \epsilon_{\Lambda} |\Lambda_{\alpha\beta\gamma}\rangle \langle \Lambda_{\alpha\beta\gamma}|, \quad (8)$$

where ϵ_{Λ} is the energy eigenvalue corresponding to the state labeled Λ , and (ii) expanding $|\Lambda_{\alpha\beta\gamma}\rangle$ in a single-center, orthonormal basis. As suggested in Fig. 1, these single-center basis states are the eigenstates of the atom that is centered at the origin. These eigenstates are also obtained from the opti-

mized potential method of density functional theory [30,34]. Expanding in this way can give a decent approximation for only compact molecules [27]. The response model used in the ion-atom collision problem [31] is incompatible with this description of the molecular problem and cannot be used.

In practice, only the minimal-basis set of initially occupied molecular orbitals was used in Eq. (8) for each target. In other words, contributions from excited and continuum states are neglected in the spectral representation of $\hat{h}_{\alpha\beta\gamma}^T$.¹ While this was not found to be problematic for high impact energies [26–28], initial results on capture for the present analysis showed inconsistencies with previous measurements [15,35]. These initial results are discussed in Sec. III A. For now, we argue that this issue can be alleviated by using a closure approximation on $\hat{h}_{\alpha\beta\gamma}^T$ [27] such that

$$\hat{h}_{\alpha\beta\gamma}^T \approx \sum_{\Lambda}^{\text{occupied}} (\epsilon_{\Lambda} - \bar{\epsilon}) |\Lambda_{\alpha\beta\gamma}\rangle \langle \Lambda_{\alpha\beta\gamma}| + \bar{\epsilon}, \quad (9)$$

where $\bar{\epsilon}$ is the average energy that represents the unoccupied molecular states. In this way, we include these states in a global fashion without burdening the computations. The choice of $\bar{\epsilon}$ is discussed in Sec. III A.

The single-particle molecular TDSE (5) solution is obtained in the same fashion as outlined in Ref. [27]. The basis set contains all states of the KLM shells of the atomic oxygen (H_2O) and carbon atom (CH_4). The same set of atomic states from $n = 2$ to $n = 6$ of the O^{5+} ion and analogous sets of TC-BGM pseudostates as for the O^{6+} -Ar system were used for the molecular problem.

Solving the single-particle TDSE yields single-particle capture probabilities into the projectile p^{cap} and target ionization probabilities p^{ion} . Within the IEM, these probabilities can be combined using multinomial analyses. For ion-molecule collisions, the single-particle probabilities are orientation averaged before multinomial calculations are carried out. Once a multinomial analysis is used, capture cross sections can be calculated by

$$\sigma = 2\pi \int_0^{\infty} b P_{\text{cap}}(b) db, \quad (10)$$

where P_{cap} denotes the capture probability obtained after performing a multinomial calculation. In the following, we describe the multinomial statistics that were used for the postcollision analysis.

B. Postcollision analysis

Machacek *et al.* [15] reported measurements and CTMC calculations on total SEC, DEC, and TEC cross sections for each collision system. These total capture cross sections include contributions from higher-multiple-capture events which undergo autoionization. We refer to these contributions as *apparent* capture. The CTMC cross sections are reported to include up to sixfold capture. To obtain these total cross sections in a feasible manner, we utilize the same

multinomial analysis used in Ref. [23] for up to sixfold capture. This involves using the *ad hoc* Auger decay scheme proposed by Ali *et al.* [36] to determine the initial configurations that result in one, two, or three electrons before undergoing radiative decay. Once all possible capture configurations are determined, we calculate P_{k_2, \dots, k_M} [23], where

$$P_{k_2, \dots, k_M} = \binom{K}{k_2 + \dots + k_M} \dots \binom{k_2 + k_3}{k_2} \times (p_2)^{k_2} \dots (p_M)^{k_M} (\tilde{p})^{\tilde{K}}, \quad (11)$$

with

$$\tilde{p} = 1 - \sum_n p_n, \quad (12)$$

$$\tilde{K} = K - k_2 - k_3 - \dots - k_M \quad (13)$$

is the probability of finding k_2 electrons in the $n = 2$ state of the projectile, k_3 electrons in the $n = 3$ state, and so forth up to the M th state. The capture probabilities p_n are averaged over the initially occupied shells. For all targets, we neglect capture from the innermost target shell since results showed these contributions are negligible. Including them would lead to crude averaging. The parameter K is the number of active electrons in the target, and k_n is the number of electrons captured into the n th state of the projectile, where $n = 2, \dots, 6$. By using Eq. (11) and the Auger decay scheme of Ali *et al.* [36], we can calculate total SEC, DEC, and TEC cross sections.

The next postcollision process to consider is radiative decay on the projectile due to SEC. To carry out this analysis, we require nl -state populations as initial conditions. One disadvantage of the *ad hoc* Auger decay scheme of Ref. [36] is that it does not provide l -subshell populations. An approach that can give the nl populations within the IEM is using the nl -specific q -fold capture with simultaneous k -fold ionization probability P_{nl}^{qk} [37,38] coupled with an *ab initio* Auger decay analysis. Since we are interested only in capture with no ionization, we refer to P_{nl}^{q0} as *pure* q -fold capture. For pure SEC, we have

$$P_{nl}^{10} = \sum_{q_1, \dots, q_m} \prod_{i=1}^m \binom{N_i}{q_i} [p_i^{\text{cap}}(n, l)]^{q_i} \times (1 - p_i^{\text{cap}} - p_i^{\text{ion}})^{N_i - q_i} \delta_{1, \sum_i q_i}, \quad (14)$$

where m is the number of initially occupied shells of the target, N_i is the number of electrons in the i th shell, and $p_i^{\text{cap}} = \sum_{n, l} p_i^{\text{cap}}(n, l)$.

The CTMC radiative spectra results by Machacek *et al.* [15] include contributions from apparent SEC. To include these contributions in the present study, we carry out an *ab initio* Auger decay analysis involving nl populations from multiple capture and add them to the pure SEC nl populations before performing the radiative-decay calculations. As one can see from Eq. (14), calculations of nl -specific capture probabilities can become difficult to manage when working with higher-multiple-capture events. However, from the *ad hoc* Auger decay analysis [36] and using Eq. (11), results show that the apparent SEC contributions are mainly from DEC. We refer to these capture events as *autoionizing double capture*

¹As explained in the Appendix of Ref. [27], the spectral representation is used only in a partial matrix element calculation.

(ADC). Contributions from higher-multiple-capture events toward apparent SEC were found to be negligible. This means that it is sufficient to carry out pure q -fold capture calculations up to $q = 2$ to account for ionization.

The corresponding P_{nl}^{qk} for nl DEC can also be calculated using Eq. (14) but with $q = 2$ and replacing the Kronecker delta with $\delta_{2, \sum_i q_i}$. DEC into nl can be calculated in a similar fashion, but the details are more involved since a larger variety of contributions have to be combined.

With the pure DEC results calculated, we multiply them by branching ratios corresponding to the Auger decay rates to extract the nl -specific ADC cross sections. These decay rates were obtained by using the AUGER component of the RATIP program [39]. In this component, the interelectronic interaction in the Auger transition amplitude calculations is described by instantaneous Coulomb repulsion, which is sufficient for light and medium elements [39]. For consistency with the IEM framework, calculations of these rates were restricted to single configurations since the program utilizes the multiconfiguration Dirac-Fock method by default.

With a full set of nl cross sections as initial populations, we calculate the probabilities of producing emission lines from radiative decay using branching ratios obtained from radiative-decay rates. The RATIP program [39] was also utilized to calculate the electric-dipole ($E1$) transition rates with the EINSTEIN component. These emission probability calculations are performed in the same manner as in Refs. [5,25]. For capture into O^{5+} ($n = 4$), the radiative cascade produces photoemission energies that correspond to the soft x-ray regime approximately from 60 to 110 eV (or to wavelengths between 10 and 20 nm).

III. RESULTS AND DISCUSSION

A. Capture cross sections

Initial TC-BGM results of the capture cross sections for the molecular targets (i.e., without the closure approximation) showed substantial differences from previous experimental results. For instance, initial results for H_2O at $E_P = 1.17$ keV/amu yield a total pure SEC of 70.33×10^{-16} cm² and that the main capture channel is O^{5+} ($n = 5$). This is inconsistent with the measurements by Bodewits and Hoekstra [35], where the main capture channel was found to be O^{5+} ($n = 4$) with a total pure SEC cross section of $(28 \pm 1.6) \times 10^{-16}$ cm² at 1.31 keV/amu. Similar inconsistencies were also found for CH_4 and at $E_P = 2.33$ keV/amu when compared with measurements by Machacek *et al.* [15]. These results for the molecular targets motivate the use of the closure approximation for the Hamiltonian (9).

Varying $\bar{\epsilon}$ in the closure approximation of $\hat{h}_{\alpha\beta\gamma}^T$ showed changes to the capture cross sections for the two molecular targets. Starting from $\bar{\epsilon} = 0$, using a negative $\bar{\epsilon}$ did not yield improved cross sections. The total pure SEC remained overestimated. However, it was found that using a small positive $\bar{\epsilon}$ yields cross sections that are more consistent with previous results. Figure 2 illustrates how the pure SEC cross section changes with respect to $\bar{\epsilon}$ for O^{6+} - H_2O and $-CH_4$ collisions at 1.17 keV/amu. The plot shows minima at $\bar{\epsilon} \approx 0.15$ and 0.125 for H_2O and CH_4 , respectively, at this

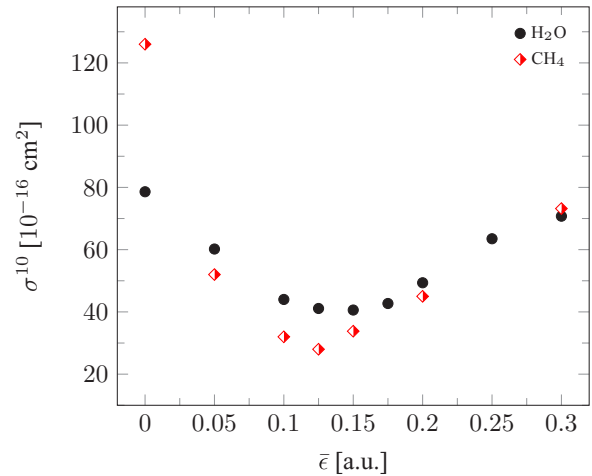


FIG. 2. Orientation-averaged pure SEC cross sections of O^{6+} - H_2O and $-CH_4$ collisions plotted with respect to the average energy of the unoccupied orbitals in the closure approximation. Calculations are for $E_P = 1.17$ keV/amu.

impact energy. The minima also occur around the same $\bar{\epsilon}$ for both molecules at $E_P = 2.33$ keV/amu.

From the perspective of sensitivity analysis, $\bar{\epsilon}$ is treated as a “perturbative” parameter in the present numerical problem. This means that a poor choice of $\bar{\epsilon}$ in the model can yield results that are significantly different from the expected solution. Therefore the $\bar{\epsilon}$ at the minimum (Fig. 2) would be the natural choice for the optimal solution since small changes of this parameter around this region do not seem to affect the solution significantly. In other words, it is the least sensitive to this particular choice.

Further examination of $\bar{\epsilon}$ around the minima in Fig. 2 reveals how differently the capture cross sections are distributed across the n states. We illustrate this change for H_2O in Table I. For this analysis, we extended the basis set by including the $n = 7$ and $n = 8$ states of the projectile. Starting with $\bar{\epsilon} = 0$, which is simply the initial calculation without the closure approximation, the n distribution shows that the main capture channel is $n = 5$, as mentioned earlier. By using $\bar{\epsilon} = -0.3$, results led to even larger total pure SEC cross sections compared to those using $\bar{\epsilon} = 0$. Interestingly, these results show that $n = 6$ is the dominant capture channel

TABLE I. Orientation-averaged n -state pure SEC cross sections (in 10^{-16} cm²) from O^{6+} - H_2O collisions at $E_P = 1.17$ keV/amu.

n state	$\bar{\epsilon}$			
	-0.3	0	0.15	0.3
2	<0.001	<0.001	<0.001	<0.001
3	0.001	0.24	2.46	10.79
4	1.25	16.18	35.76	59.64
5	11.88	51.00	0.73	0.01
6	50.01	0.95	0.04	0.06
7	40.89	0.12	0.02	0.04
8	22.83	0.85	0.02	0.09
Total	126.86	70.33	39.03	70.63

and that capture is generally shifted towards higher excited states compared to $\bar{\epsilon} = 0$. Moving towards a positive $\bar{\epsilon}$ of 0.15, calculations yield a total pure SEC which is similar to measurements by Bodewits and Hoekstra [35] and show that the main capture channel is $n = 4$, consistent with predictions using the OBM [16,17]. Although results using $\bar{\epsilon} = 0.3$ also show the main capture channel of O^{5+} ($n = 4$), the total pure SEC cross section is much larger than measurements from Bodewits and Hoekstra [35]. This shows that the use of such $\bar{\epsilon}$ is inappropriate and that $\bar{\epsilon} = 0.15$ would, indeed, be the optimal choice, as suggested by the sensitivity analysis argument. Similar results were also found for CH_4 , except that the minimum occurs at $\bar{\epsilon} \approx 0.125$. From here on out, capture cross sections from collisions with molecular targets are based on results obtained using the optimal $\bar{\epsilon}$ in the closure approximation.

Figure 3 displays the pure SEC probabilities plotted with respect to the impact parameter. Only capture probabilities into $n = 4$ of the projectile are shown since it is the main capture channel and curves from other states are negligible in comparison. Starting with capture from Ar [Fig. 3(a)], there is considerable enhancement in capture in the response model compared to the no-response approximation. This is a reflection of the decrease in electron screening of the target core that is included in the response model.

Next, with capture from H_2O [Fig. 3(b)], one can see similarities in the probabilities between the two orientations at small impact parameters, but their differences are pronounced between $b = 10$ and $b = 15$. Specifically, a high capture probability is present at these impact parameters when H_2O is at the (0,0,0) orientation with both hydrogen atoms lying in the scattering plane. Although the orientation averaging may seem crude at first glance because of the substantial differences between the two orientations, it turns out that by including other orientation results in the averaging, one obtains a nearly identical profile of the probability curve and thus similar cross sections. This is illustrated in Appendix A.

As for CH_4 [Fig. 3(c)], the probability curves for the different orientations are very similar to each other. The only exception to this is the (45,90,180) orientation where capture probabilities between $b = 10$ and $b = 15$ are relatively high compared to the other three orientations. This can be understood from its geometry, in which two of the hydrogen atoms lie in the xz half plane with $x > 0$ such that the projectile moves by at closer proximity than for the other orientations.

Total capture cross sections for each collision system are shown in Table II. The cross sections include contributions from autoionizing multiple capture based on the analysis using the *ad hoc* Auger decay scheme by Ali *et al.* [36]. The present TC-BGM results are compared with measurements and CTMC results reported by Machacek *et al.* [15].

For O^{6+} -Ar, there are notable differences in total capture cross sections between the TC-BGM no-response and response model calculations for both impact energies. The latter results are closer in agreement with the experiment than the former and CTMC as well. While the TC-BGM response results are not within the uncertainty range of the experimental measurements, even for TEC, the discrepancies are on the 20% level. By contrast, the CTMC results for TEC are underestimated by

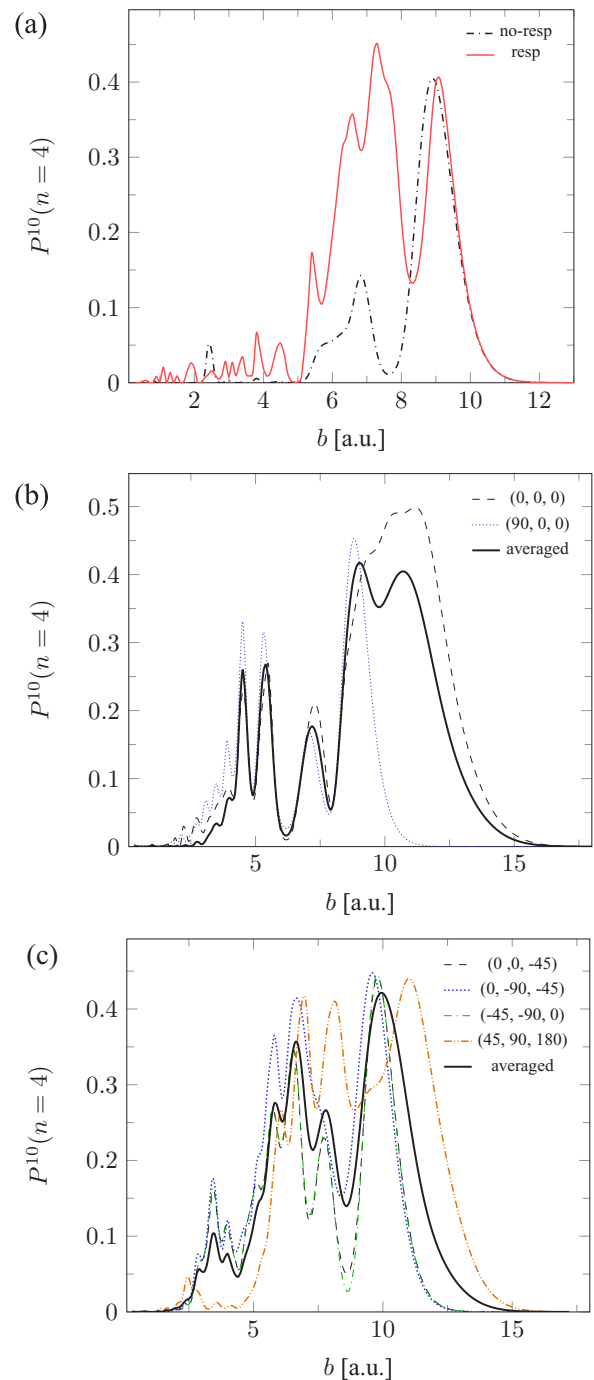


FIG. 3. TC-BGM pure SEC probabilities for O^{5+} ($n = 4$) plotted with respect to the impact parameter at $E_p = 1.17$ keV/amu. Calculations are for the following targets: (a) Ar, showing no-response and response curves, (b) H_2O , showing two orientations and the orientation-averaged results, and (c) CH_4 , showing four orientations and the orientation-averaged results.

an order of magnitude with respect to the experimental results for both impact energies. This underestimation of CTMC TEC cross sections can also be seen for all other targets studied in Ref. [15].

For O^{6+} - H_2O , we see some similarities in cross sections between the TC-BGM and experimental data for both impact

TABLE II. Total SEC, DEC, and TEC cross sections (in 10^{-16} cm²) in O⁶⁺-Ar, -H₂O, and -CH₄ collisions. The present TC-BGM results are shown along with experimental and CTMC results by Machacek *et al.* [15].

O ⁶⁺ -Ar		TC-BGM		Expt. [15]	CTMC [15]
E_p (keV/amu)		No response	Response		
1.17	SEC	29.6	46.5	49.8 ± 3.4	59.0
	DEC	19.4	10.4	8.4 ± 0.6	5.44
	TEC	5.82	3.47	2.9 ± 0.2	0.126
2.33	SEC	30.3	44.5	46.5 ± 3.1	63.2
	DEC	17.1	8.76	7.1 ± 0.5	5.60
	TEC	6.32	2.64	2.2 ± 0.2	0.138
O ⁶⁺ -H ₂ O					
E_p (keV/amu)		TC-BGM		Expt. [15]	CTMC [15]
1.17	SEC	59.7		47.3 ± 3.2	55.0
	DEC	15.5		8.3 ± 0.6	6.30
	TEC	4.57		3.7 ± 0.3	0.580
2.33	SEC	58.1		45.9 ± 3.1	57.4
	DEC	12.9		7.4 ± 0.5	6.53
	TEC	3.18		2.6 ± 0.2	0.586
O ⁶⁺ -CH ₄					
E_p (keV/amu)		TC-BGM		Expt. [15]	CTMC [15]
1.17	SEC	52.7		42.9 ± 2.9	54.2
	DEC	26.6		17.8 ± 1.3	6.76
	TEC	4.94		2.7 ± 0.2	0.659
2.33	SEC	50.9		50.2 ± 3.4	56.7
	DEC	23.2		16.3 ± 1.2	6.94
	TEC	4.30		2.3 ± 0.2	0.634

energies. However, the TC-BGM DEC results are somewhat overestimated relative to the experiment and CTMC. When examining the present cross sections for each individual multiple-capture configuration, we find that triple capture into the $n = 4$ state has the largest contribution to the apparent DEC cross section. Regardless, this did not appear to be problematic for the calculation of the total TEC cross section, for which quite satisfactory agreement with the measurement is found.

Last, for O⁶⁺-CH₄, the present TC-BGM cross sections are also seen to be in satisfactory agreement with the experimental data [15] for both impact energies. Although the present DEC cross sections appear relatively large, they are in better agreement with the experiment than CTMC. Overall, the present TC-BGM results are consistent with the measurements by Machacek *et al.* [15] in that the total capture cross sections do not vary significantly for each collision system at solar wind speeds due to the similar ionization energies of the targets.

With the total capture cross-section analysis complete, we now focus the discussion on cross sections relevant to the radiative cascade analysis. Given that the outcome of the radiative cascade is dependent on the initial populations of the nl states, it is worthwhile to examine these populations for each collision system. Table III displays the $3l$ and $4l$ distributions of total SEC (pure SEC and ADC using the multinomial analyses) for each collision system. The present results show that ADC mainly contributes to capture into the $n = 2$ and $n = 3$ shells of O⁵⁺. Contributions to SEC for $n = 4$ due to ADC were found to be negligible. A similar table listing the pure SEC $3l$ distributions is given in Appendix B to illustrate the role of ADC.

There are some similarities and differences in the nl distribution for each collision system. For instance, capture into lower l states for $n = 4$ is seen to be large from all targets. In other words, the $4l$ populations do not resemble a statistical distribution [i.e., $\propto (2l + 1)$], an observation that is generally

TABLE III. TC-BGM SEC nl distribution (in 10^{-16} cm²) for O⁶⁺-Ar, -H₂O, and -CH₄ collisions. Results include both pure SEC and ADC.

States (n, l)	Ar		H ₂ O	CH ₄
	No response	Response		
$E_p = 1.17$ keV/amu				
3, 0	0.44	4.04	1.59	0.78
3, 1	0.99	2.54	1.17	2.28
3, 2	2.33	0.99	2.44	4.34
4, 0	6.29	16.3	16.13	11.0
4, 1	4.04	5.95	9.98	9.18
4, 2	1.44	2.13	2.93	3.71
4, 3	3.31	4.73	6.29	6.18
$E_p = 2.33$ keV/amu				
3, 0	0.48	3.23	2.21	0.66
3, 1	0.91	1.48	1.54	1.79
3, 2	3.76	1.87	3.10	5.60
4, 0	6.20	8.56	10.2	7.81
4, 1	3.31	4.31	7.90	5.96
4, 2	2.20	2.71	5.41	3.96
4, 3	4.37	5.96	6.38	5.50

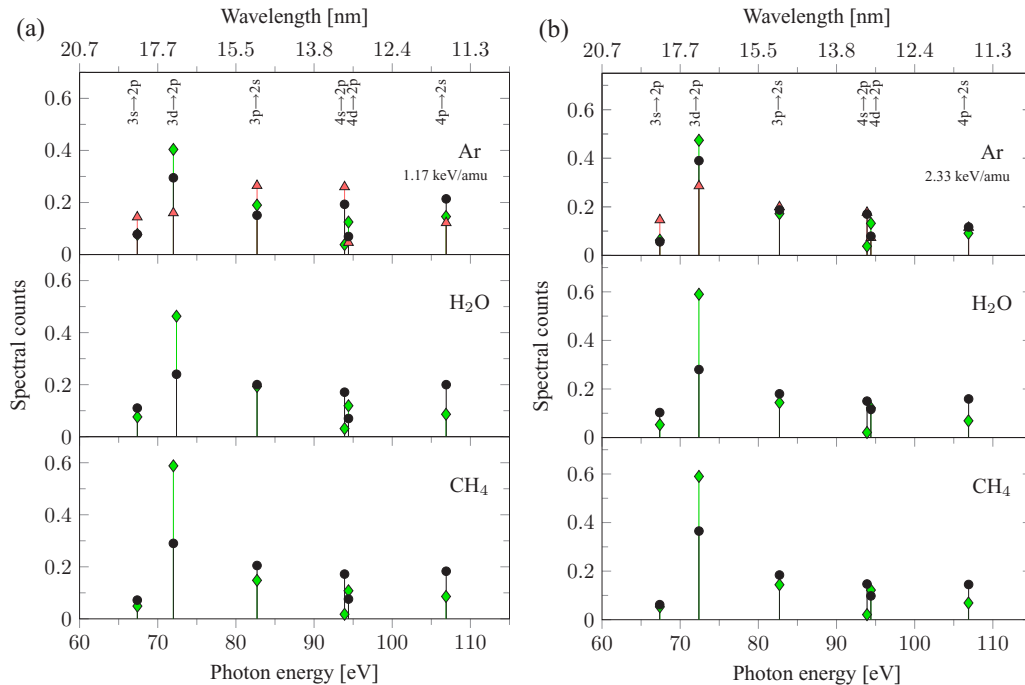


FIG. 4. Calculated emission spectra for O^{6+} -Ar, $-H_2O$, and $-CH_4$ collisions at impact energies of (a) 1.17 keV/amu and (b) 2.33 keV/amu. Calculations are CTMC results by Machacek *et al.* [15] (\blacklozenge), the present results using the TC-BGM in the no-response approximation (\bullet), and the present results using the response model (\blacktriangle). Note that the wavelength scale shown at the top of each group plot does not scale linearly.

seen at low impact energies [16,40]. This is also consistent with measurements by Bodewits and Hoekstra [35] for collisions with H_2O . In addition, we see that these nl cross sections do not vary significantly between the two impact energies with the exception of the $4s$ state, where there is a noticeable decrease at 2.33 keV/amu.

Further inspection of the nl distributions for Ar in Table III shows that the capture cross section for $4s$ is the largest and that the result from the response model is almost three times larger than the no-response approximation at 1.17 keV/amu. This result appears to be unexpected since previous TC-BGM studies suggest the response model would enhance capture in the maximum l state [24,25]. This might be due to the projectile not being a bare ion in the present study, which has the consequence that the energy degeneracy of the l states is lifted such that higher l states have lower ionization energies than lower l states.

B. Radiative spectra

Figure 4 displays the calculated emission spectra due to total SEC (pure SEC and ADC) from the present TC-BGM and previous CTMC calculations [15] of all collision systems considered in this study. Figure 4(a) shows the spectra at an impact energy of 1.17 keV/amu, while Fig. 4(b) shows the spectra at 2.33 keV/amu. To compare the present results with CTMC [15], the spectral counts from each set of calculations are normalized to unity. Furthermore, Fig. 5 shows the Grotrian diagram for the O^{5+} ion with all the transitions from Fig. 4 included.

By examining Fig. 4, one can see that the spectra between the two collision energies exhibit similar patterns. In particular, the $3d \rightarrow 2p$ transition line has the largest count. The

only exception to this observation is the present response calculation for Ar at 1.17 keV/amu [top panel of Fig 4(a)]. Looking at the nl capture cross sections for target Ar in Table III, it can be seen that capture into $3d$ is relatively small compared to $3s$ in the response calculation. On the other hand, we see the $3d \rightarrow 2p$ line is increased for 2.33 keV/amu, where capture is more probable at the maximum l state for both $n = 3$ and $n = 4$ (Table III). This tendency was also seen from the spectra measurements of Bodewits and Hoekstra [35] for O^{6+} - H_2O collisions.

Continuing with the discussion of the $3d \rightarrow 2p$ transition line, one can see that the CTMC results for this line are

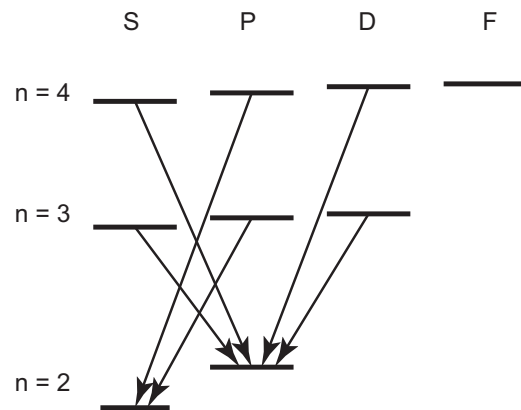


FIG. 5. Grotrian diagram for the O^{5+} ion. The arrows from one energy level to another indicate the radiative-decay transitions. The transitions shown in the diagram are those for which spectral counts are shown in Fig. 4. They are assumed to follow the electric-dipole selection rule.

larger than the TC-BGM results, especially for the molecular targets. Since information for the partial cross sections were not reported by Machacek *et al.* [15], we look at the spectral measurements by Miller *et al.* [2] to help guide the present comparisons between the two calculated spectra. This measurement is for O^{6+} -CO collisions at $E_p \approx 2$ keV/amu.

Given that the CO molecule has a first ionization energy of 14.01 eV, the OBM expectation is that the main capture channel is O^{5+} ($n = 4$). Therefore we expect that the resulting spectra due to SEC into O^{6+} closely resemble those shown in Fig. 4(b). From the measurements by Miller *et al.* [2], it was found that the normalized intensity count for the $3d \rightarrow 2p$ transition line is 0.43 ± 0.09 . The corresponding present TC-BGM results for Ar, H_2O , and CH_4 at 2.33 keV/amu are 0.41, 0.28, and 0.38, respectively. If the emission spectra for the O^{6+} -CO collisions measured by Miller *et al.* [2] are a good representation of the three present targets, then the implication is that the present H_2O spectral count for the $3d \rightarrow 2p$ transition line is underestimated, while the CTMC calculation is overestimated since both results lie outside of the uncertainty range of the measurement. From the Grotrian diagram (Fig. 5), one can infer that the capture cross sections for $3d$ are underestimated by the TC-BGM. Since $4f$ can also contribute to this line in the cascade, it is possible that the cross section for $4f$ could be underestimated as well.

There are also other differences in spectral counts for other transitions that one can see in Fig. 4, such as the $4p \rightarrow 2s$ transition line. However, these differences appear to be less prominent than those for the spectral counts of the $3d \rightarrow 2p$ line. One can also carry out similar comparisons for the other spectral lines in Fig. 4(b) with the measurements by Miller *et al.* [2] and find that both the TC-BGM and CTMC results are mostly within the uncertainty range. As Machacek *et al.* [15] suggested, however, a more appropriate confirmation of these predicted emission spectra would have to come from new measurements on the collision systems considered in the present study. Nevertheless, the present TC-BGM analysis reaffirms the conclusion by Machacek *et al.* [15] that the total capture cross sections and corresponding emission spectra vary only slightly with the target species considered.

IV. CONCLUSIONS

In this study we presented an analysis based on the IEM framework using the TC-BGM to describe electron capture and its resulting emission spectra in O^{6+} -Ar, $-H_2O$, and $-CH_4$ collisions at 1.17 and 2.33 keV/amu impact energies. The present results were mainly benchmarked with experimental and theoretical results by Machacek *et al.* [15].

The present analysis of O^{6+} -Ar collisions showed that the response model results are more consistent with the total capture measurements by Machacek *et al.* [15] than the no-response approximation. While emission spectra from the response model appeared to be consistent overall with CTMC calculations and no-response results for 2.33 keV/amu, that was not the case for the lower impact energy. This is mostly due to the differences in how the response model predicts the nl distributions compared to the no-response approximation. While it was concluded in previous BGM studies [24,25] that the response model would enhance the maximum l -state

population, that tendency is not seen in the present case of the projectile not being a bare ion.

The TC-BGM capture cross sections for the molecular targets were initially shown to be inconsistent with previous results. Specifically, the initial results were (i) vastly overestimated and (ii) did not predict the correct main capture channel on the projectile. For these reasons, we utilized a closure approximation in the spectral representation of the molecular Hamiltonian and found that this had a significant impact on capture cross-section results. With this technique, we showed that it is possible, at least for H_2O and CH_4 , to perform a quantum-mechanical analysis that can reliably describe slow ion-molecule collisions within the IEM framework.

ACKNOWLEDGMENTS

The work presented in this article was funded by the Natural Sciences and Engineering Research Council of Canada (NSERC) under Grant No. RGPIN-2014-03611. High-performance computing resources for this work were provided by the Shared Hierarchical Academic Research Computing Network (SHARCNET). A.C.K.L. gratefully acknowledges the financial support provided by the Ontario Graduate Scholarship, which is jointly funded by the Province of Ontario and York University (Canada).

APPENDIX A: ORIENTATION DEPENDENCE OF H_2O CROSS-SECTION CALCULATIONS

In Sec. III A, we presented results of the pure SEC probability as a function of the impact parameter for H_2O at $E_p = 1.17$ keV/amu [Fig. 3(b)]. The plot shows a noticeable difference in capture for the molecular orientations considered in the present study, (0,0,0) and (90,0,0). We illustrate that including results from other orientations in the averaging leads to very similar results in the total capture cross-section calculation.

Figure 6 shows the pure SEC probability results plotted with respect to the impact parameter for six orientations of

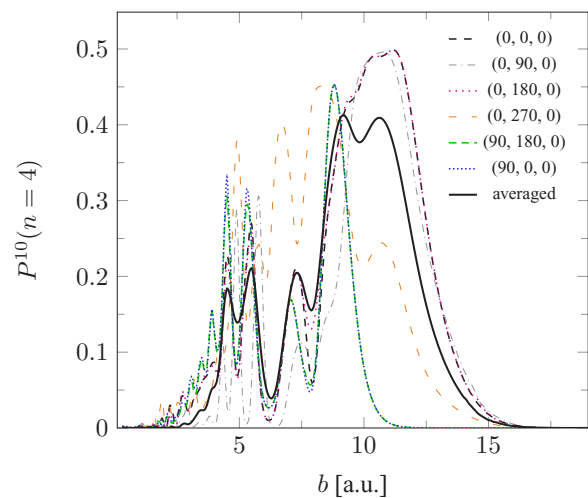


FIG. 6. TC-BGM pure SEC probabilities for O^{5+} ($n = 4$) from collision with H_2O plotted with respect to the impact parameter at $E_p = 1.17$ keV/amu.

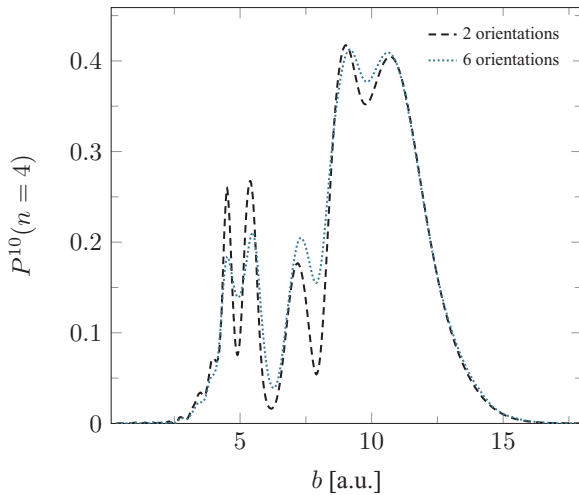


FIG. 7. TC-BGM pure SEC probabilities for O^{5+} ($n = 4$) from collisions with H_2O plotted with respect to the impact parameter at $E_p = 1.17$ keV/amu. The “2 orientations” label refers to $(0,0,0)$ and $(90,0,0)$, while the “6 orientations” label refers to those in Fig. 6.

H_2O . The plot also shows the averaged results based on these six orientations. From Fig. 6, we see that the curves of $(0,90,0)$ and $(0,180,0)$ have profiles very similar to that of $(0,0,0)$. This can be understood from the fact that in these three orientations the hydrogen atoms lie in the scattering plane. This is also true for $(0,270,0)$, but the position of the hydrogen atoms for this orientation would be the farthest from the projectile, which likely explains the lower capture probabilities for $b > 10$. Likewise, the $(90,180,0)$ curve has a profile nearly identical to that of $(90,0,0)$ since the hydrogen atoms lie in the azimuthal plane.

TABLE IV. TC-BGM $3l$ partial pure SEC cross sections (in 10^{-16} cm 2).

States (n,l)	Ar			
	No response	Response	H_2O	CH_4
$E_p = 1.17$ keV/amu				
3, 0	0.07	3.94	1.36	0.10
3, 1	0.27	2.35	0.73	1.08
3, 2	0.10	0.47	0.37	0.52
$E_p = 2.33$ keV/amu				
3, 0	0.17	3.10	1.79	0.15
3, 1	0.31	1.21	1.11	0.89
3, 2	0.16	0.52	0.50	0.42

We now compare the orientation-averaged result of H_2O in Fig. 6 with the averaged result in Fig. 3(b). Figure 7 shows these orientation-averaged results for O^{5+} ($n = 4$) at $E_p = 1.17$ keV/amu. Clearly, the two averaged curves have a very similar profile. By calculating the capture cross section for each averaged curve in Fig. 7 we obtain 36.65×10^{-16} cm 2 for averaging all six orientations, compared with a very similar result of 35.53×10^{-16} cm 2 for averaging the two orientations of $(0,0,0)$ and $(90,0,0)$. Therefore we see that averaging the $(0,0,0)$ and $(90,0,0)$ results is just as sufficient as averaging over all six orientations of H_2O .

APPENDIX B: PARTIAL CROSS-SECTION DATA

In Sec. III A, results of the nl partial capture cross sections based on contributions from both pure SEC and ADC were discussed. Table IV lists the $3l$ partial capture cross sections from only pure SEC.

- [1] R. Ali, P. Beiersdorfer, C. L. Harris, and P. A. Neill, *Phys. Rev. A* **93**, 012711 (2016).
- [2] K. A. Miller, W. W. Smith, T. Ehrenreich, Q. C. Kessel, E. Pollack, C. Verzani, V. A. Kharchenko, A. Chutjian, J. A. Lozano, N. Djuric, and S. J. Smith, *Astrophys. J.* **742**, 130 (2011).
- [3] R. J. Mawhorter, J. B. Greenwood, A. Chutjian, T. Haley, C. D. Mitescu, and J. Simcic, *Phys. Rev. A* **84**, 052714 (2011).
- [4] R. K. Smith, A. R. Foster, and N. S. Brickhouse, *Astron. Nachr.* **333**, 301 (2012).
- [5] M. Fogle, D. Wulf, K. Morgan, D. McCammon, D. G. Seely, I. N. Draganić, and C. C. Havener, *Phys. Rev. A* **89**, 042705 (2014).
- [6] C. M. Lisse, K. Dennerl, J. Engenhauser, M. Harden, F. E. Marshall, M. J. Mumma, R. Petre, J. P. Pye, M. J. Ricketts, J. Schmitt, J. Trumper, and R. G. West, *Science* **274**, 205 (1996).
- [7] T. E. Cravens, *Geophys. Res. Lett.* **24**, 105 (1997).
- [8] N. A. Schwadron and T. E. Cravens, *Astrophys. J.* **544**, 558 (2000).
- [9] T. R. Kallman and P. Palmeri, *Rev. Mod. Phys.* **79**, 79 (2007).
- [10] A. R. Foster, L. Ji, H. Yamaguchi, R. K. Smith, and N. S. Brickhouse, *AIP Conf. Proc.* **1545**, 252 (2013).
- [11] R. K. Smith and N. S. Brickhouse, *Adv. At. Mol. Opt. Phys.* **63**, 271 (2014).
- [12] V. A. Krasnopolsky, *Icarus* **247**, 95 (2015).
- [13] R. Olson, *Springer Handbook of Atomic, Molecular, and Optical Physics* (Springer, New York, 2006), pp. 869–874.
- [14] W. Fritsch and C. D. Lin, *J. Phys. B* **19**, 2683 (1986).
- [15] J. R. Machacek, D. P. Mahapatra, D. R. Schultz, Y. Ralchenko, A. Moradmand, M. O. A. El Ghazaly, and A. Chutjian, *Astrophys. J.* **809**, 75 (2015).
- [16] H. Ryufuku and T. Watanabe, *Phys. Rev. A* **20**, 1828 (1979).
- [17] A. Niehaus, *J. Phys. B* **19**, 2925 (1986).
- [18] M. Zapukhlyak, T. Kirchner, H. J. Lüdde, S. Knoop, R. Morgenstern, and R. Hoekstra, *J. Phys. B* **38**, 2353 (2005).
- [19] S. Knoop, M. Keim, H. J. Lüdde, T. Kirchner, R. Morgenstern, and R. Hoekstra, *J. Phys. B* **38**, 3163 (2005).
- [20] M. Zapukhlyak, T. Kirchner, A. Hasan, B. Tooke, and M. Schulz, *Phys. Rev. A* **77**, 012720 (2008).
- [21] G. Schenk, M. Horbatsch, and T. Kirchner, *Phys. Rev. A* **88**, 012712 (2013).
- [22] T. Kirchner, N. Khazai, and L. Gulyás, *Phys. Rev. A* **89**, 062702 (2014).
- [23] A. Salehzadeh and T. Kirchner, *J. Phys. B* **46**, 025201 (2013).
- [24] A. C. K. Leung and T. Kirchner, *Phys. Rev. A* **92**, 032712 (2015).

- [25] A. C. K. Leung and T. Kirchner, *Phys. Rev. A* **93**, 052710 (2016).
- [26] H. J. Lüdde, T. Spranger, M. Horbatsch, and T. Kirchner, *Phys. Rev. A* **80**, 060702 (2009).
- [27] M. Murakami, T. Kirchner, M. Horbatsch, and H. J. Lüdde, *Phys. Rev. A* **85**, 052704 (2012).
- [28] M. Murakami, T. Kirchner, M. Horbatsch, and H. J. Lüdde, *Phys. Rev. A* **86**, 022719 (2012).
- [29] A. Salehzadeh and T. Kirchner, *Eur. Phys. J. D* **71**, 66 (2017).
- [30] E. Engel and S. H. Vosko, *Phys. Rev. A* **47**, 2800 (1993).
- [31] T. Kirchner, M. Horbatsch, H. J. Lüdde, and R. M. Dreizler, *Phys. Rev. A* **62**, 042704 (2000).
- [32] R. M. Pitzer and D. P. Merrifield, *J. Chem. Phys.* **52**, 4782 (1970).
- [33] R. M. Pitzer, *J. Chem. Phys.* **46**, 4871 (1967).
- [34] J. D. Talman and W. F. Shadwick, *Phys. Rev. A* **14**, 36 (1976).
- [35] D. Bodewits and R. Hoekstra, *Phys. Rev. A* **76**, 032703 (2007).
- [36] R. Ali, C. L. Cocke, M. L. A. Raphaelian, and M. Stockli, *Phys. Rev. A* **49**, 3586 (1994).
- [37] T. Kirchner, H. J. Lüdde, and R. M. Dreizler, *Phys. Scr.* **T80**, 416 (1999).
- [38] M. Horbatsch, *Phys. Rev. A* **49**, 4556 (1994).
- [39] S. Fritzsche, *Comput. Phys. Commun.* **183**, 1525 (2012).
- [40] R. Janev and H. Winter, *Phys. Rep.* **117**, 265 (1985).